A Novel Hybrid Brain-Computer Interface Combining Motor Imagery and Intermodulation Steady-State Visual Evoked Potential

Xinyi Chi, Chunxiao Wan, Chunyan Wang, Yong Zhang, Xiaogang Chen, *Member, IEEE*, and Hongyan Cui

***Abstract*— The hybrid brain-computer interface (hBCI) combining motor imagery (MI) and steady-state visual evoked potential (SSVEP) has been proven to have better performance than a pure MI- or SSVEP-based brain-computer interface (BCI). In most studies on hBCIs, subjects have been required to focus their attention on flickering light-emitting diodes (LEDs) or blocks while imagining body movements. However, these two classical tasks performed concurrently have a poor correlation. Therefore, it is necessary to reduce the task complexity of such a system and improve its user-friendliness. Aiming to achieve this goal, this study proposes a novel hybrid BCI that combines MI and intermodulation SSVEPs. In the proposed system, images of both hands flicker at the same frequency (i.e., 30 Hz) but at different grasp frequencies (i.e., 1 Hz for the left hand, and 1.5 Hz for the right hand), resulting in different intermodulation frequencies for encoding targets. Additionally, movement observation for subjects can help to perform the MI task better. In this study, two types of brain signals are classified independently and then fused by a scoring mechanism based on the probability distribution of relevant parameters. The online verification results showed that the average accuracies of 12 healthy subjects and 11 stroke patients were 92.40 ± 7.45% and 73.07 ± 9.07%, respectively. The average accuracies of 10 healthy subjects in the MI, SSVEP, and hybrid tasks were 84.00 ± 12.81%, 80.75 ± 8.08%, and 89.00 ± 9.94%, respectively. The high recognition accuracy verifies the feasibility and robustness of the proposed system. This study provides a novel and natural paradigm for a hybrid BCI based on MI and SSVEP.**

***Index Terms*— Brain-computer interface, motor imagery, steady-state visual evoked potential, intermodulation frequency.**

I. Introduction

BRAIN-COMPUTER interface (BCI), which can establish a communication and control pathway between the brain and an external environment independent of peripheral nerves or muscles, has been one of the most active research directions in the field of neural engineering [1]. The BCI can help to restore the self-care ability of individuals with movement disorders. Electroencephalography (EEG) has been a common brain imaging technique for building a BCI system because it has the advantages of high time resolution and being non-invasive and portable. Currently, steady-state visual evoked potential (SSVEP) and motor imagery (MI) have been widely studied in EEG-based BCIs [2], [3].

A hybrid BCI, which incorporates multiple signals containing at least one cerebral signal into a BCI system to improve its practicality and performance, has been another popular research direction in the field of neural engineering [4]. In the existing studies on a hybrid BCI, the SSVEP has been one of the most commonly used brain signals. The SSVEP is an evoked EEG response generated over the occipital area focusing on the periodic visual stimulus at a specific frequency [5]. It has characteristics of time-locking and phase-locking and can be evoked stably in most people under high signal-to-noise ratio (SNR) and information transfer rate (ITR)[6]. Significant progress has been made in the development of stimulation methods [7]–[10], classification algorithms [11]–[13], and applications [14], [15] of the SSVEP-BCI, providing a great potential to construct hybrid BCIs using different signals. The MI has been another classical paradigm used in the research on hybrid BCIs. The MI activates distinct patterns in the corresponding areas of the sensorimotor cortex by mentally simulating the movement of different body parts. [16]. The commands in the MI-BCI share a strong correlation with the movement intention [17]–[19]. However, due to the low spatial

Manuscript received November 18, 2021; revised February 28, 2022 and April 19, 2022; accepted May 31, 2022. Date of publication June 3, 2022; date of current version June 10, 2022. This work was supported in part by the National Natural Science Foundation of China under Grant 62171473, in part by the Key-Area Research and Development Program of Guangdong Province under Grant 2018B030339001, and in part by the Fundamental Research Funds for the Central Universities under Grant 3332019015. *(Xinyi Chi and Chunxiao Wan contributed equally to this work.) (Corresponding authors: Xiaogang Chen; Hongyan Cui.)*

This work involved human subjects or animals in its research. Approval of all ethical and experimental procedures and protocols was granted by the Ethical Committee of Tianjin Medical University General Hospital under Approval No. IRB2021-YX-096-01, Dated May 27, 2021.

Xinyi Chi, Xiaogang Chen, and Hongyan Cui are with the Institute of Biomedical Engineering, Chinese Academy of Medical Sciences and Peking Union Medical College, Tianjin 300192, China (e-mail: xinyi_bboy@163.com; chenxg@bme.cams.cn; cokey1981@hotmail.com).

Chunxiao Wan, Chunyan Wang, and Yong Zhang are with Tianjin Medical University General Hospital, Rehabilitation Medicine, Tianjin 300052, China (e-mail: wcx2226@163.com; dip4@163.com; doctoryongzhang@126.com).

Digital Object Identifier 10.1109/TNSRE.2022.3179971

resolution of the EEG and physiological mechanism of the MI, it is challenging to extend the command set size of a pure MI-BCI under the premise of reliable performance. The MI illiteracy has the highest proportion of BCI illiteracy. Most people could not perform a MI task well for the first time [6].

In recent years, a hybrid MI+SSVEP-BCI based on the asynchronous and synchronous modes has been proposed. In the asynchronous mode, the MI and SSVEP tasks are performed sequentially. The superiority of this mode reflects in the diversity of commands and simplicity of operation in the application. Hence, a command set based on the serial fusion of MI and SSVEP has been commonly used for external devices to achieve more complex operations [20]–[24]. In contrast, in the synchronous mode, the MI and SSVEP tasks are performed simultaneously. Allison *et al.* [25], [26] introduced a MI+SSVEP hybrid BCI paradigm that subjects performed the left- or right-hand motion imagery while focusing on the ipsilateral LED. They proved that the hybrid BCI could help to improve accuracy and reduce the number of BCIs illiteracy. Yu *et al.* [27] emphasized the auxiliary effect of the SSVEP on the MI. They expected merging SSVEP into MI-BCI could provide feedback that could reflect subjects' intentions more accurately. Ko *et al.* [28] believed that the addition of SSVEP features could compensate for the performance decline caused by the reduction in the number of electrodes used in the system. Yang *et al.* [29] proposed a synchronized hybrid BCI system to recognize a total of 10 mental tasks, i.e., an idle state, a single MI mode, four single SSVEP modes, and four hybrid MI+SSVEP modes, via two EEG channels. In these studies, frequencies of visual stimuli were all below 20 Hz for strong SSVEPs. However, this might cause visual fatigue and even photosensitive epileptic seizures [30]. A higher-frequency stimulus (above 25 Hz) induces a weaker SSVEP, whereas the signal-to-noise rate (SNR) might not decrease significantly [31]. Additionally, a higher stimulus frequency is considered to provide better comfort and security. Moreover, flickering blocks with uniform brightness or LEDs were used as stimuli and therefore a weak correlation between MI and SSVEP tasks in these studies. Also, obvious flashes might distract subjects, thus bringing difficulties in performing the movement imagery.

In this study, an innovative hybrid BCI paradigm based on the intermodulation frequency coding approach [32], which combines the MI and SSVEP synchronously, is proposed. The flickering images of hand grasping are used instead of flickering blocks or arrows with uniform brightness. This latter approach has been widely used in the SSVEP-related research. Furthermore, a high-frequency stimulation is selected for improving system comfort. In the stimulation, both hands grasped at different speeds to evoke distinguishable intermodulation SSVEPs. Subjects were instructed to focus their attention on a specific target hand image while imagining the corresponding hand movement. The proposed system provided movement observation to help the subjects to perform a MI task [33], [34]. The MI and SSVEP signals extracted from their dominant brain regions were classified separately, and a fusion decision was made by the proposed scoring mechanism. Considering the potential of the MI-BCI in rehabilitation [35], the feasibility of the proposed system is verified by online experiments with not only healthy individuals but stroke patients. In addition, an online comparative experiment containing a movement imagery task under the MI condition, a visual task under the SSVEP condition, and a fusion task under the hybrid condition, was conducted to compare the performance between the proposed hybrid paradigm and two single modality paradigms. The objective results have been presented via the classification accuracy and the subjective results have been obtained via questionnaires.

The rest of this paper is organized as follows. In Section II, materials and methods are described. The results are presented in Section III. The performances of the proposed hybrid BCI are discussed in Section IV. Finally, the conclusions are drawn in Section V.

II. Methods And Materials

A. Experimental Environment

1) Subjects: This study involved an offline experiment for parameter optimization, an online verification experiment, and an online comparative experiment. Fourteen healthy subjects (three males and 11 females, aged from 20 years to 27 years, with a mean age of 24 years) participated in the offline experiments. None of the subjects had prior experience with a MI- or SSVEP-based BCI. Twelve healthy subjects (three males and nine females, aged from 21 years to 28 years, with a mean age of 24 years) participated in the online verification experiments. Eight of them also participated in the offline experiments. Eleven stroke patients (nine males and two females, aged from 34 years to 85 years, with a mean age of 62 years) also took part in the online verification experiment. Furthermore, ten healthy subjects (two males and eight females, aged from 22 years to 30 years, with a mean age of 25 years) participated in the online comparative experiment. Four of them joined the online verification experiment, while the others were inexperienced in using the proposed hybrid BCI or even had no prior experience with any BCI-related experiment. All subjects had normal or corrected-to-normal vision. The subjects were neither suffering from neurological or psychiatric disorders nor taking medications known to adversely affect the EEG recording. All subjects read and signed a written informed consent before the experiment and were paid for their participation. The ethical committee of Tianjin Medical University General Hospital approved this study.

2) Stimulus Design: The visual stimulus was presented on an LCD monitor of 24 inches, with a 60-Hz refresh rate and a screen resolution of 1,920 $\times$1,080. The user interface contained two images of both hands with a size of 716 $\times$ 597 pixels. During the experiment, the left- and right-hand images switched between the closed and open states at different rates, providing an impression that the hands were grasping. Meanwhile, pictures changed between the hand images and a black image to provide a visual flicker stimulation. The stimulus program was developed using the Psychophysics Toolbox Version 3 of MATLAB (MathWorks, Inc.) software [36].

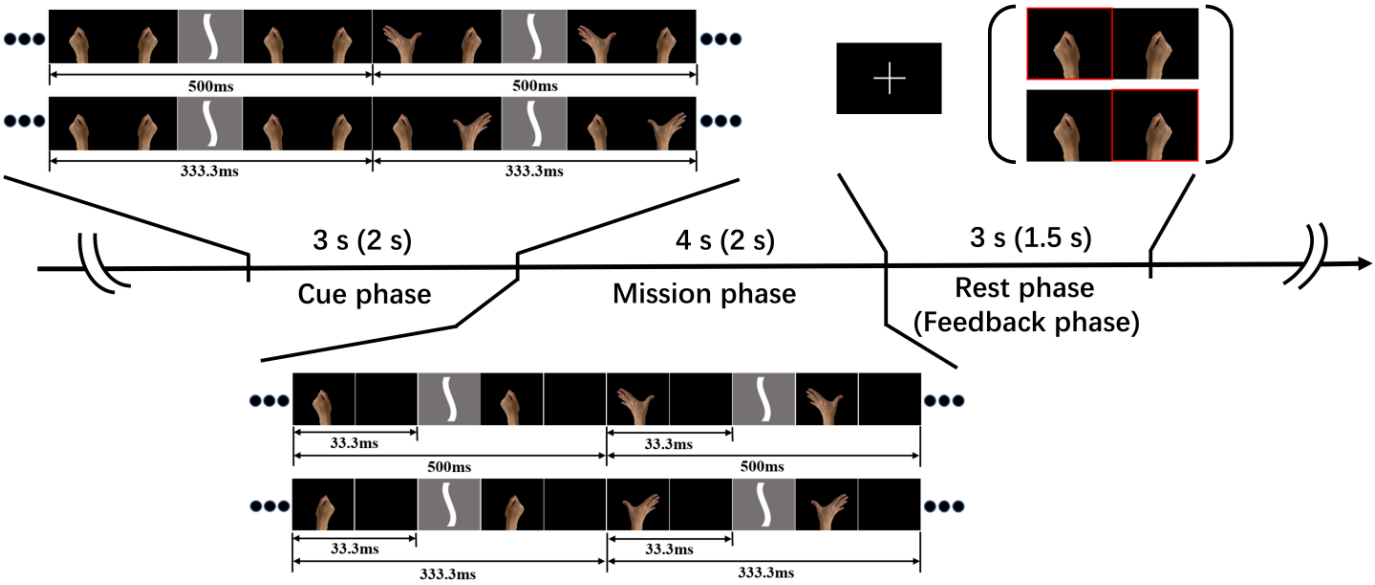

Fig. 1. The offline and online experimental procedures. A complete trial of the offline experiment included three phases: cue phase (3 s), mission phase (4 s), and resting phase (3 s). A complete trial of the online experiment included three phases: cue phase (2 s), mission phase (2 s), and resting or feedback phase (1.5 s).

3) Data Acquisition: The subjects were seated comfortably in front of the monitor at a viewing distance of approximately 70 cm. A Synamps2 system (Neuroscan, Inc.) was used to non-invasively record the scalp EEG signals. Sixty electrodes in the 64-channel modified international 10-20 system excluding M1, M2, CB1, and CB2 were used in the offline experiment. According to the offline analysis, only 30 electrodes were used in the online experiment, of which 22 electrodes, including FC3, FC1, FCz, FC2, FC4, C3, C1, Cz, C2, C4, CP3, CP1, CPz, CP2, CP4, P5, P3, P1, Pz, P2, P4, and P6, were used to obtain the MI-EEG, and nine electrodes, including Pz, PO5, PO3, POz, PO2, PO4, O1, Oz, and O2, were used to obtain the SSVEP-EEG. The left mastoid was selected as a reference electrode, and the ground electrode was placed between Fz and FPz. All electrode impedances were maintained below 10 kΩ. Raw EEG data were band-pass filtered between 0.15 Hz and 100 Hz, notch filtered at 50 Hz, and sampled at 1 kHz. In the online experiment, the EEG data and event triggers were sent from the data acquisition device to the stimulation device via TCP/IP protocol and then were analyzed to provide the feedback in real-time.

B. Experimental Design

1) Offline Experiment: The offline experiment included eight blocks, each of which consisted of 20 trials, namely 10 trials for the left hand and 10 trials for the right hand. In each block, the trials were presented in the pseudo-randomized order, and each trial lasted for 10 s. Also, each trial consisted of three phases: cue phase, mission phase, and resting phase. In the cue phase that lasted 3 s, images of closed left- and right-hand were displayed on the screen first. Then, an image of a certain hand started to alternate between the closed and opened statuses at a specific frequency; for the left hand, the frequency was 1 Hz, and for the right hand, the frequency was 1.5 Hz. In this way, a visual impression that one hand was grasping while the opposite hand remained closed was created. This was a cue for target selection in the next phase. In the mission phase, each hand began to grasp at the corresponding frequency, as mentioned above, and simultaneously, images of both hands flickered at a frequency of 30 Hz. The subjects needed to concentrate on a particular hand image on the screen following the cue in the cue phase and performing a movement imagination of this hand in the mission phase, which lasted 4 s. Muscle tension should be avoided, and the subjects were asked to perform first-person kinesthetic rather than visual MI when performing tasks [37]. Then, a white cross was presented for 3 s in the resting phase, providing a break between trials. There is a break of an uncertain time between blocks depending on the subjects' mental state. The offline experimental procedure is shown in Fig. 1.

2) Online Verification Experiment: The online verification experiment consisted of training and test stages. The training stage included three blocks, each of which included 20 trials, 10 trials for the left hand, and 10 trials for the right hand. The training data were used to calculate the spatial filter and classification model. Each trial included the cue, mission, and resting phases, which lasted for 2 s, 2 s, and 1.5 s, respectively. No feedback was provided in the training stage. The test stage consisted of four blocks, each of which included 20 trials, and was used to evaluate the feasibility of the proposed system. In the test stage, the resting phase of the training stage was replaced by the feedback phase. The cue phase, the mission phase, and the feedback phase lasted for 2 s, 2 s, and 1.5 s, respectively. The EEG signal was analyzed in real-time to provide the visual feedback on a red wireframe surrounding the target after the mission phase. The online verification experimental procedure is also shown in Fig. 1.

3) Online Comparative Experiment: The online comparative experiment consisted of 12 blocks. In the two SSVEP blocks, the subjects performed only the visual task on the flickering

hand grasp images. In the five MI blocks, the subject performed the movement imagery task; the former three blocks were used for training, and the latter two blocks with the feedback were used for the test. In the five fusion blocks, the subject performed the fusion task, the same as in the online verification experiment; the former three blocks were used for training, and the latter two blocks with the feedback were used for the test. Each block contained 20 trials, and the cue, task, and resting/feedback phases in each trial lasted for 2 s, 2 s, and 1.5 s, respectively. Note that a white cross would appear during the resting phase in the training stage, and a red wireframe surrounding one of the targets would appear during the feedback phase in the test stage.

After the experiment, each subject was asked to fulfill a questionnaire consisting of three questions by answering on a scale from one to five [25]. The first question was: "Did you find the flickering lights annoying?"; the offered answers included: "Not Annoying at All," "Slightly Annoying," "Annoying," "'Relatively Annoying," and "Very Annoying," which corresponded to 1–5 on the scale, respectively. The second and the third question were respectively: "Did you find it difficult to image the hand movements?" and "Did you find the hybrid condition more difficult than the other two conditions?"; the offered answers to both questions were: "Very Easy," "Easy," "Neither Easy nor Difficult," "Difficult," and "Very Difficult," which corresponded to 1–5 on the scale, respectively.

C. Signal Processing Algorithm

1) MI Signal Processing: The collected MI signal was processed after being down-sampled to 250 Hz and band-pass filtered in the range between 8 Hz and 30 Hz. Tikhonov regularized common spatial-spectral pattern (TRCSSP), which combined Tikhonov regularized common spatial pattern (TRCSP) [38] and common spatial-spectral pattern (CSSP) [39], was used to analyze the MI signal. Assume $\boldsymbol{X^k} \in \mathbb{R}^{N_{chm} \times N_p}$ denote the preprocessed MI signal of the kth trial, where N_{ch_m} is the number of channels used in the MI signal analysis, and N_p is the number of sample points; $C^k \in \{1; 2\}$ represents the label of the kth trial, where "1" indicates left, and "2" indicates right. A time-delayed matrix $\delta^\tau \boldsymbol{X}^k$ was appended to $\boldsymbol{X}^k$ as additional channels, which can be expressed by,

$$\hat{\boldsymbol{X}}^k = \left(\frac{\boldsymbol{X}^k}{\delta^\tau \boldsymbol{X}^k}\right), \tag{1}$$

where δ^τ denotes a delay operator for notational convenience, and it is defined by,

$$\delta^\tau \left(\boldsymbol{X}_{.,t}\right) = \boldsymbol{X}_{.,t-\tau}, \tag{2}$$

where τ is a user-defined parameter representing the delay time.

The two class-covariance matrices can be expressed by:

$$\boldsymbol{\Sigma}_1 = < \hat{\boldsymbol{X}}^k \hat{\boldsymbol{X}}^{k^T} >_{\{k:C^k=1\}}, \tag{3}$$

$$\boldsymbol{\Sigma}_2 = < \hat{\boldsymbol{X}}^k \hat{\boldsymbol{X}}^{k^T} >_{\{k:C^k=2\}}, \tag{4}$$

where T denotes transpose. To learn spatial filters $\boldsymbol{\omega}$ that maximize the variance of bandpass-filtered MI signal from class 1 (i.e., $\boldsymbol{\Sigma}_1$) while minimizing those from class 2 (i.e., $\boldsymbol{\Sigma}_2$), the following objective function was constructed using Tikhonov regularization and the penalty function $P(\boldsymbol{\omega}) = \|\boldsymbol{\omega}\|_2^2$:

$$J_{P_1}(\boldsymbol{\omega}) = \frac{\boldsymbol{\omega}^T \boldsymbol{\Sigma}_1 \boldsymbol{\omega}}{\boldsymbol{\omega}^T \boldsymbol{\Sigma}_2 \boldsymbol{\omega} + \alpha P(\boldsymbol{\omega})} = \frac{\boldsymbol{\omega}^T \boldsymbol{\Sigma}_1 \boldsymbol{\omega}}{\boldsymbol{\omega}^T (\boldsymbol{\Sigma}_2 + \alpha \boldsymbol{I}) \boldsymbol{\omega}}. \tag{5}$$

Then, the eigenvalue problem derived from (5) was defined by:

$$(\boldsymbol{\Sigma}_2 + \alpha \boldsymbol{I})^{-1} \boldsymbol{\Sigma}_1 \boldsymbol{\omega} = \lambda \boldsymbol{\omega}. \tag{6}$$

The filters $\boldsymbol{\omega}_1$ maximizing $J_{P_1}(\boldsymbol{\omega})$ denoted eigenvectors corresponding to the largest eigenvalues of $\boldsymbol{M}_1 = (\boldsymbol{\Sigma}_2 + \alpha \boldsymbol{I})^{-1} \boldsymbol{\Sigma}_1$. However, the eigenvectors corresponding to the lowest eigenvalues of $\boldsymbol{M}_1$ minimized $J_{P_1}(\boldsymbol{\omega})$ and thus maximized the penalty function. To obtain filters $\boldsymbol{\omega}_2$ that maximized $\boldsymbol{\Sigma}_2$ while minimizing $\boldsymbol{\Sigma}_1$, another objective function was defined as follows:

$$J_{P_2}(\boldsymbol{\omega}) = \frac{\boldsymbol{\omega}^T \boldsymbol{\Sigma}_2 \boldsymbol{\omega}}{\boldsymbol{\omega}^T (\boldsymbol{\Sigma}_1 + \alpha \mathbf{I}) \boldsymbol{\omega}}. \tag{7}$$

Filters $\boldsymbol{\omega}_2$ denoted the eigenvectors corresponding to the largest eigenvalues of $\boldsymbol{M}_2 = (\boldsymbol{\Sigma}_1 + \alpha \boldsymbol{I})^{-1} \boldsymbol{\Sigma}_2$. Finally, the spatial filters $\boldsymbol{W}$ denoted eigenvectors corresponding to m_0 largest eigenvalues of $\boldsymbol{M}_1$ and m_0 largest eigenvalues of $\boldsymbol{M}_2$. Using this spatial matrix $\boldsymbol{W}$, the MI signal $\hat{\boldsymbol{X}}^k$ were projected by $\boldsymbol{W}$ as follows:

$$\boldsymbol{Z}^k = \boldsymbol{W} \hat{\boldsymbol{X}}^k = \boldsymbol{W}^{(0)} \boldsymbol{X}^k + \boldsymbol{W}^{(\tau)} \delta^\tau \boldsymbol{X}^k, \tag{8}$$

where $\boldsymbol{Z}^k \in \mathbb{R}^{2m_0 \times 2N_{chm}}$ denotes the projected matrices; columns of $\boldsymbol{W}$ were divided in two submatrices: $\boldsymbol{W}^{(0)}$ that applied to $\boldsymbol{X}^k$, and $\boldsymbol{W}^{(\tau)}$ that applied to the delayed channels $\delta^\tau \boldsymbol{X}^k$.

The feature $\boldsymbol{feature}^k$ used for the training and classification was obtained by:

$$\boldsymbol{feature}^k = log\left(var\left(\boldsymbol{Z}^k\right)\right), \tag{9}$$

where $\boldsymbol{feature}^k$ is a vector containing $2m_0$ elements representing the feature of the kth trial. Then a support vector machine (SVM) with a linear kernel function was used as a classification model.

2) SSVEP Signal Processing: The collected SSVEP signal was processed after being band-pass filtered in the range between 20 Hz and 100 Hz. The filter-bank canonical correlation analysis (FBCCA) was used to analyze the SSVEP signal [11].

Assume $\boldsymbol{Y}^k \in \mathbb{R}^{N_{ch_s} \times N_p}$ denoted the preprocessed SSVEP signal of the kth trial, where N_{ch_s} is the number of channels used in the SSVEP signal analysis. First, the SSVEP signal was processed by multiple zero-phase Chebyshev-type-I infinite impulse response (IIR) filters with different passbands. Next, sub-band components $\boldsymbol{Y}^k_{SB_n}, n = 1, 2, \ldots, N$ were obtained. Then, the canonical correlation analysis (CCA) was performed on the SSVEP sub-band components and reference signals $\boldsymbol{R}^C, C \in \{1, 2\}$; $\boldsymbol{R}^C$ denotes a matrix containing a series of sine-cosine signals whose frequencies correspond to the characteristic frequencies that may appear in SSVEP

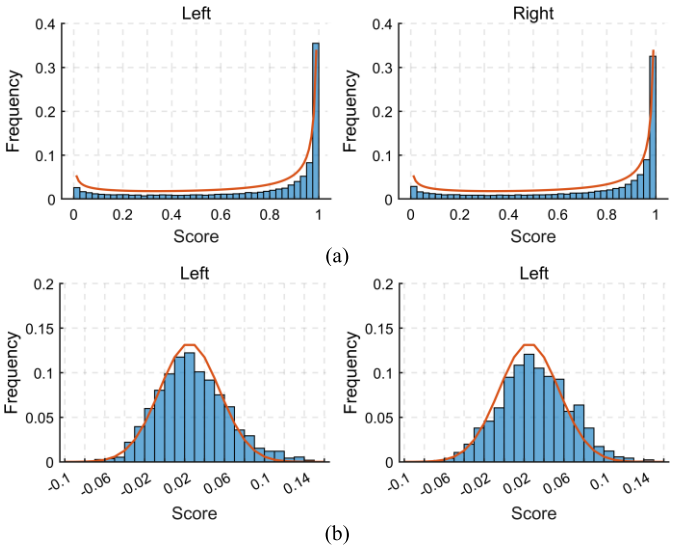

Fig. 2. Statistical distributions and the corresponding probability distributions with a similar trend. (a) Statistical distributions of parameters obtained by the MI algorithm sharing a similar trend with the beta distribution; (b) Statistical distributions of parameters obtained by the SSVEP algorithm sharing a similar trend with the normal distribution.

signals of class C. The characteristic frequencies represent linear combinations of the flicker frequency f_z and hand grasping rate f_l or f_r. After performing the CCA between reference signals $\boldsymbol{R}^C$ corresponding to class C and all sub-band components of $\boldsymbol{Y}^k$, a set of Pearson correlation coefficients $\rho_1^C, \rho_2^C, \ldots, \rho_N^C$ was obtained:

Then, a weighted sum of squares of the correlation values corresponding to all sub-band components was calculated for the target identification: $\tilde{\rho^C} = \sum_{n=1}^{N} w(n) \cdot (\rho_n^C)^2$; $w(n)$ denotes a user-defined weight for the sub-band components, and it holds that $w(1) + w(2) = 1$. By comparing $\tilde{\rho^1}$ and $\tilde{\rho^2}$, the class of $\boldsymbol{Y}^k$ could be identified.

3) Fusion Method: In the MI signal processing, SVM classification model identified the class of test features from the MI signals by comparing the score for each class. In the offline data processing, the score of left- and right-handed MI signals outputted by the classification model in the procedure of cross-validation were obtained, and its probability distribution was simulated. Details about the cross-validation process are given in Section III. The MATLAB function $fitcsvm$ was used to train the model while function $predict$ was used to classify MI signal. By default, the output scores of classes are opposite to each other. They were standardized and shifted using the function of $f(x) = 1/\left(1 + e^{-2x}\right)$ to satisfy the condition of $b_1, b_2, 0 < b_1, b_2 < 1$. The statistical and probability distributions are presented in Fig. 2(a), where it can be seen that the beta distribution $g(x \mid \alpha_m, \beta_m)$ was used for the simulation of the statistical distribution, which can be expressed by:

$$g(x|\alpha_m, \beta_m) = \frac{x^{\alpha_m - 1}(1-x)^{\beta_m - 1}}{B(\alpha_m, \beta_m)}, 0 < x, \alpha_m, \beta_m < 1, \tag{10}$$

$$B(\alpha_m, \beta_m) = \int_0^1 x^{\alpha_m - 1}(1-x)^{\beta_m - 1}\, dx. \tag{11}$$

In the SSVEP signal processing, the FBCCA generates two values, $e_1$ande_2, for the classification of a single trial, which denote the correlation coefficients between the SSVEP signal and two target templates. The difference between these two values was analyzed, and a normal probability distribution $h(x|\mu, \sigma^2)$ was used to simulate the statistical distribution as shown in Fig. 2(b) and expressed by:

$$h\left(x \mid \mu, \sigma^2\right) = \frac{1}{\sqrt{2\pi}\sigma} e^{-\frac{(x-\mu)^2}{2\sigma^2}}, -\infty < x < +\infty. \tag{12}$$

The proposed fusion method is to calculate the possibilities p_1 and p_2 that a single test trial falls into the two categories, and $p_{1(2)} = p_{1(2)}{}^{MI} * p_{1(2)}{}^{SSVEP}$, where:

$$p_{1(2)}^{MI} = G\left(b_{1(2)}|\alpha_m, \beta_m\right) \Big/ p^{MI}, \tag{13}$$

$$p^{MI} = G(b_1|\alpha_m, \beta_m) + G(b_2|\alpha_m, \beta_m), \tag{14}$$

$$p_{1(2)}^{SSVEP} = H\left(e_{1(2)} - e_{2(1)}|\mu, \sigma^2\right) \Big/ p^{SSVEP}, \tag{15}$$

$$p^{SSVEP} = H\left(e_1 - e_2|\mu, \sigma^2\right) + H\left(e_2 - e_1|\mu, \sigma^2\right), \tag{16}$$

where G and H denote the cumulative distribution functions of g and h, respectively. The final class was determined by comparing p_1 and p_2.

The architecture of the overall signal processing algorithm is illustrated in Fig. 3.

III. Results

A. Parameter Optimization

1) MI: Reasonable channel optimization aims to improve the classification accuracy of a MI-BCI. Considering the dominant brain region of MI signal and symmetry of channel distribution, the classification performance of MI signal was evaluated and compared using several channel sets. The whole data containing 160 trials, each of which had a data length of 4 s, was used to analyze for each subject. 22 channels were selected for the MI classification to build an online system. In addition, there were two user-defined parameters denoted by α and τ in the TRCSSP algorithm, which represented the regularization parameter and the time delay parameter, respectively. To obtain optimal values of α and τ, the final classification performance was estimated for different parameter combinations by the method of cross-validation and grid search, as shown in Fig. 4(a). Particularly, to keep consistency with subsequent analysis, 60 trials, of which 30 trials for the left hand, and 30 trials for the right hand, were used for training, and the rest 100 trials were used for the test in each round of cross-validation. Referring to the highest performance, α and τ were set to 10^{-5} and seven, respectively.

2) SSVEP: According to the visual stimulus design, the flickering frequency of f_z= 30Hz and the grasp frequencies of f_l= 1Hz for the left hand and f_r = 1.5Hz for the right hand, were set. The experimental design aimed to induce distinguishable intermodulation components for encoding two

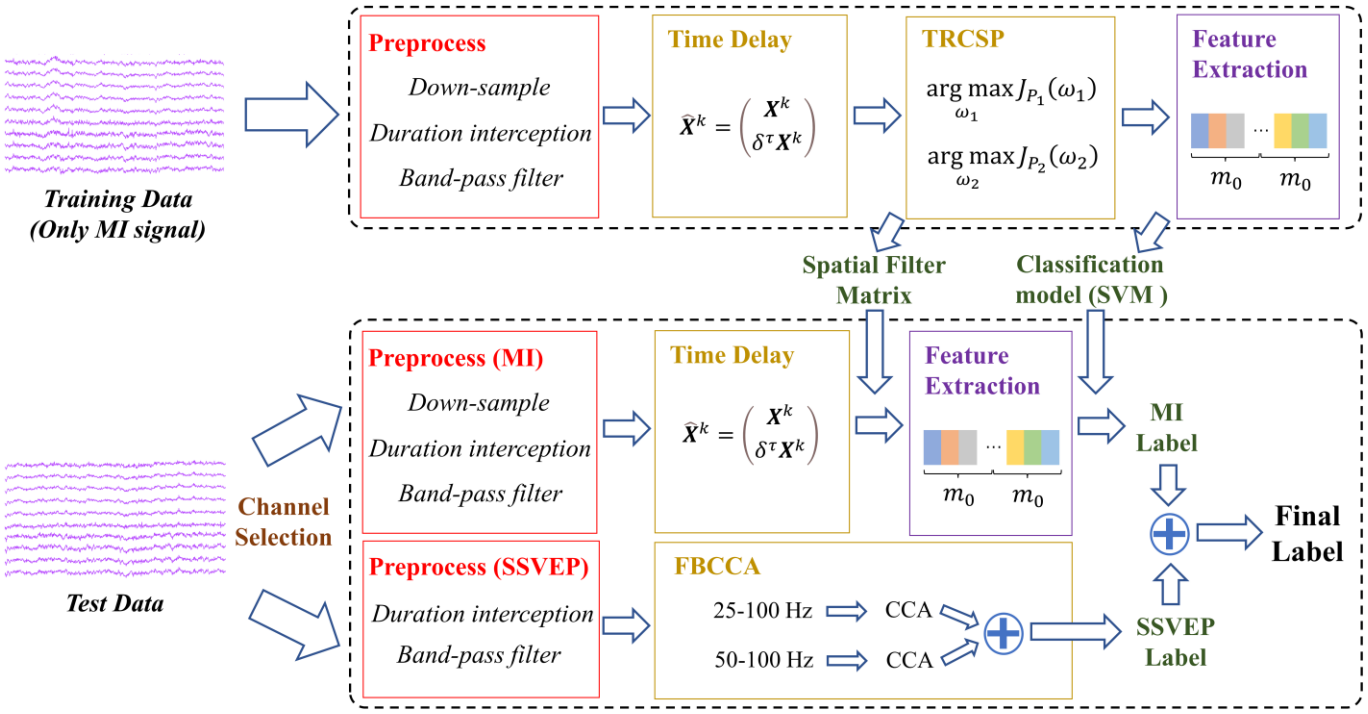

Fig. 3. The overall architecture of the proposed EEG decoding algorithm.

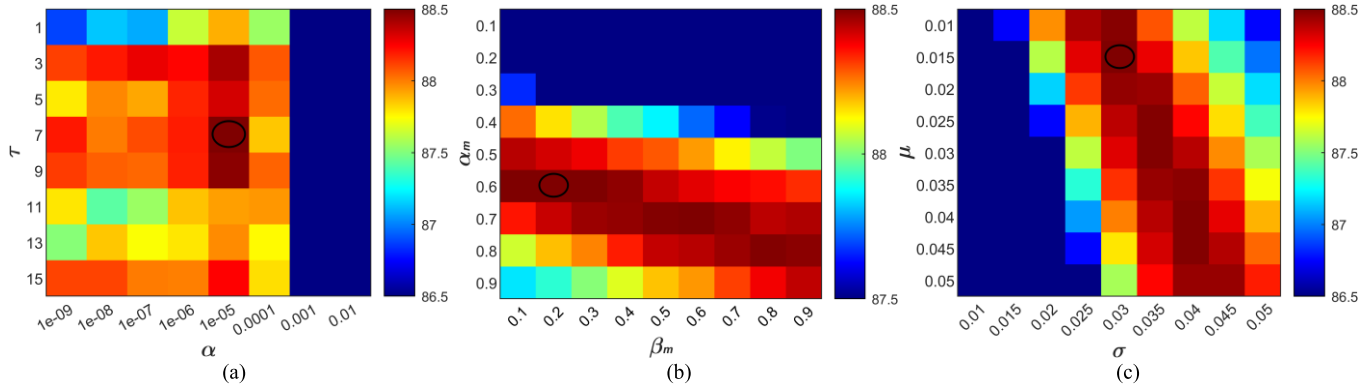

Fig. 4. Results of the grid search method and the optimal parameter values. (a) Regularization parameter α was searched in a set of $10^{-9}, 10^{-8}, \ldots, 10^{-1}$, and the time delay parameter τ was searched in a set of $1, 3, \ldots, 15$; (b) Statistical model parameters of the MI, α_m and β_m,were searched in a set of 0.1,0.2, . . . , 0.9; (c) Statistical model parameters of the SSVEP,μ and σ, were searched in 0.01,0.015, . . . , 0.05. Only part of the results is presented for a better illustration of the difference. The black ellipses indicate the location of the maximum accuracy and the corresponding selected parameters.

targets. The amplitude spectrum of the SSVEPs is presented in Fig. 5, where it can be seen that there were obvious peaks at intermodulation components of $f_z \pm f_l, 2f_z \pm f_l, f_z \pm 2f_l, 2f_z \pm 2f_l$, $f_z \pm f_r, 2f_z \pm f_r$, $f_z \pm 2f_r$, and $2f_z \pm 2f_r$. Thus, in the FBCCA method, the reference signals corresponding to these frequencies were adopted for the standard CCA. Although the SSVEP harmonics with frequencies of up to 90 Hz still showed obvious peaks, intermodulation components at $3f_z \pm nf_l$ and $3f_z \pm nf_r$ were very weak. In this study, the number of sub-bands was set to two. The frequency ranges of the two sub-bands were 25 Hz–100 Hz and 50 Hz–100 Hz. The sub-band weights $w(1) = 0.5$ and $w(2) = 0.5$ were determined by the grid search method. The results verified that the proposed experimental design could provide stable intermodulation components.

3) Fusion Method: Referring to (10) and (12), two sets of parameters (i.e., $\alpha_m, \beta_m, \mu, \sigma$) need to be determined. The optimal value of two sets of parameters were determined by the grid search method, as shown in Figs. 4(b) and 4(c). Similarly, the classification performance was obtained by the cross-validation method, as mentioned in the part about the MI parameter optimization. As shown in Figs. 4(b) and 4(c), the optimal values of $\alpha_m = 0.6, \beta_m = 0.2, \mu = 0.015, \sigma = 0.03$ were selected for the online experiment.

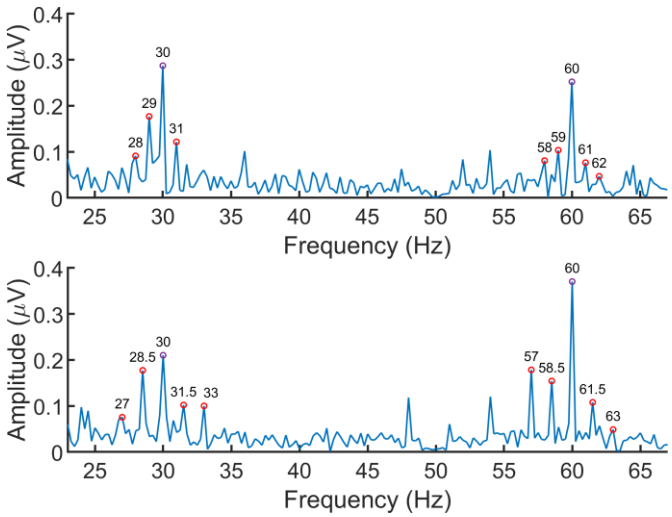

Fig. 5. The characteristic frequency peaks corresponding to the left and right hand from a representing subject. The signals from each channel and trial were averaged to perform the fast Fourier transform (FFT).

B. Offline Experiment Performance

The offline experiment consisted of eight blocks, which included a total of 160 trials. To evaluate the influence of different training set numbers on the performance, 160 trials were randomly divided into eight groups in each round of cross-validation; each group included 20 trials, 10 trials for the left hand, and 10 trials for the right hand. For a certain training set number n_g, the remaining groups $8-n_g$ were used for test. The mean accuracies of all combinations choosing n_g out of eight were calculated. The cross-validation procedure was repeated 10 times to reduce the model performance's dependence on the data division method. The relationship between the number of training sets and the classification accuracies obtained using the MI feature, the SSVEP feature, and the fusion feature separately is presented in Fig. 6(a). As shown in Fig. 6(a), the classification accuracies of the MI and fusion features increased with the number of training sets. The classification accuracy of the SSVEP feature was stable because an unsupervised algorithm was selected for the SSVEP classification. The slight change was caused by a random selection of data in the cross-validation process. One-way repeated measure analysis of variance (ANOVA) revealed that there was a significant difference in the classification accuracy of fusion ($F(6, 91) = 2.6$, $p < 0.05$). However, the difference existed only between the first and last groups; there was no significant difference between the remaining six groups. This study assumed that too many training trials might cause subjects to get tired easily. Therefore, three groups, including 60 trials, were adopted in this study. On the basis of these findings, the relationship between the data length and classification accuracies was studied further. The average accuracies obtained using the MI feature, the SSVEP feature, and the fusion feature separately for different data lengths are presented in Fig. 6(b). As shown in Fig. 6(b), the classification accuracies increased with the data length. When the data length was less than 2 s, the classification accuracies were below 80%. Fig. 6(c) illustrates the mean ITR for different data lengths. Considering that the cue and rest times could be properly adjusted as the mission time changed in the online experiment, to maintain a reasonable time distribution, an ideal ITR based only on the mission time (i.e., the data length) was calculated. When the data length reached 2 s, the ITR of fusion results achieved the maximum value. Thus, the data length of 2 s was used to construct the online system.

The fusion label was calculated using the labels and scores derived from the analysis of the MI and SSVEP signals. As shown in Figs. 6(a) and 6(b), the accuracy using fusion feature was higher than the accuracy using MI or SSVEP features. The paired t-test result revealed a significant difference in the accuracy between using the MI feature, which was 77.82 ± 9.73%, and the fusion feature, which was 88.51 ± 4.51%, under the selected number of training sets and data length ($p < 0.001$). Since there was an outlier in the accuracy when using the SSVEP feature, a Wilcoxon signed rank test was conducted for comparing accuracy using the SSVEP feature, which was 80.36 ± 11.94%, with that using the fusion feature. The result showed a significant difference in accuracy for the selected number of training sets and data length ($p < 0.05$). These results proved the effectiveness of the proposed fusion method.

TABLE I
ONLINE PERFORMANCE AND THE CORRESPONDING OFFLINE RESULTS

Subject	Offline performance (%)	Online performance (%)
S1	——	93.75
S2	——	92.50
*S3**	90.11	98.75
*S4**	92.00	78.75
S5	——	90.00
*S6**	83.86	92.50
*S7**	91.68	100.00
*S8**	96.07	96.25
*S9**	88.61	91.25
*S10**	87.43	98.75
*S11**	95.52	98.75
S12	——	77.50
Average ± SD	——	92.40 ± 7.45

Subjects marked with '*' also took part in the offline experiment.

C. Online Verification Experiment Performance

Table I lists the results of the online verification experiment of 12 healthy subjects. The average fusion accuracy achieved in the experiment was 92.40 ± 7.45%. The corresponding offline results of the subjects who participated in both offline and online verification experiments are also given in Table I. For these subjects, the paired t-test results showed that there was no obvious difference in fusion accuracy ($p = 0.22$) between the offline experiment (i.e., 90.66 ± 4.09%) and the online verification experiment (i.e., 94.38 ± 7.07%).

Table II shows the information and performance of the online verification experiment of 11 patients. The average fusion accuracy declined significantly to 73.07 ± 9.07% compared to that of healthy subjects but was still much higher than the random probability of 50%. Three patients,

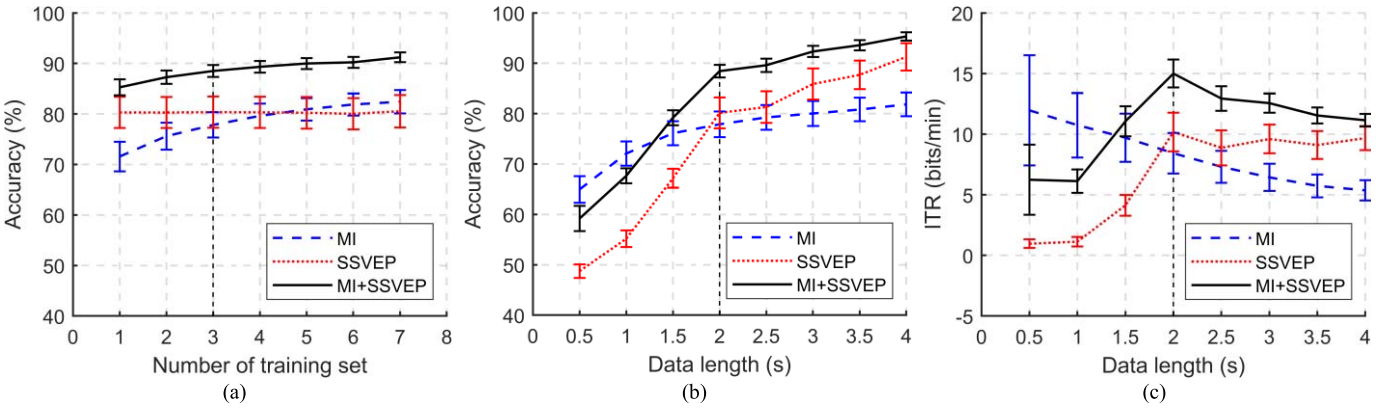

Fig. 6. The BCI performances of the MI, SSVEP, and MI+SSVEP modalities under different experimental conditions. (a) The mean accuracies for different numbers of training set samples. The error bars indicate the standard error. (b) The mean accuracies for a different data length. The error bars indicate the standard error. (c) The ITR under different data lengths from 0.5 s to 4 s with a step of 0.5 s. The ITR is maximal at the data length of 2 s. The error bars indicate the standard error.

TABLE II
INFORMATION AND ONLINE PERFORMANCE OF THE PATIENTS

Patient	Sex	Age	Diagnosis	Impairment of extremities	Online performance (%)
P1	M	34	Left cerebral hemorrhage	Right hemiparesis	81.25
P2	M	44	Right cerebral infarction	Left hemiplegia	67.50
P3	M	85	Left cerebral infarction	Right hemiparesis	62.50
P4	M	64	Right cerebral infarction	Left hemiparesis	90.00
P5	M	64	Left cerebral infarction	Right hemiparesis	62.50
P6	F	59	Left cerebral infarction	Right hemiplegia	71.25
P7	M	65	Bilateral cerebral infarction	Right hemiparesis	65.00
P8	M	66	Left cerebral infarction	Right hemiparesis	76.25
P9	M	63	Left cerebral infarction	Right hemiparesis	83.75
P10	M	69	Left cerebral infarction	Right hemiparesis	68.75
P11	F	73	Left cerebral infarction	Right hemiparesis	75.00
Average ± SD	——	62.36 ± 13.60	——	——	73.07 ± 9.07

TABLE III
ONLINE PERFORMANCE OF THE COMPARATIVE EXPERIMENT

Subject	Online performance (%)		
	MI	SSVEP	fusion
S1	90.00	80.00	92.50
S3	95.00	82.50	85.00
S10	82.50	85.00	87.50
S11	90.00	82.50	92.50
S13	92.50	90.00	100.00
S14	85.00	90.00	100.00
S15	80.00	70.00	82.50
S16	60.00	65.00	70.00
S17	100.00	77.50	100.00
S18	65.00	85.00	80.00
Average ± SD	84.00 ± 12.81	80.75 ± 8.08	89.00 ± 9.94

P1, P4, and P9, used the proposed system with an accuracy of over 80%.

D. Online Comparative Experiment Performance

Table III lists the performance of the online comparative experiment. The online performances of the MI, SSVEP, and hybrid tasks were 84.00 ± 12.81%, 80.75 ± 8.08%, and 89.00 ± 9.94%, respectively. The paired t-test results showed that there was a significant difference between the SSVEP and fusion tasks ($p < 0.01$), and there was marginally significant difference between the MI and fusion tasks ($p = 0.063$). For most of the subjects, the accuracy in the hybrid task was better than in the other two tasks.

For the hybrid task, the accuracies obtained for the MI and SSVEP features were 81.75 ± 13.95% and 79.50 ± 11.71%, respectively. The paired t-test results showed that there was no significant difference in the accuracy between the MI task and the hybrid task defined by the MI feature only ($p = 0.29$), as well as between the SSVEP task and the hybrid task defined by the SSVEP feature only ($p = 0.71$). This could indicate that the performance and signal features of a single modality task were not obviously interfered by another modality task during the hybrid task.

E. Questionnaire Results

The results of the three questions corresponding to the visual, movement-imagery, and fusion tasks were 1.70 ± 1.06, 2.2 ± 1.14, and 2.10 ± 1.10, respectively. This means the subjects generally were of the opinion that the flickering was slightly annoying and that the fusion task did not significantly increase the difficulty compared to the single modality task. Note several special score in questionnaire results, subjects S16 and S18 were inexperienced in using a BCI, and they

both answered the second question with a '4', i.e., "Difficult," and performed not that well in the movement imagery task. In addition, subject S3 reported that the flickers were relatively annoying and that the hybrid task was more difficult than the other two tasks, giving "4" to both questions. This matches the performances of S3 in performing the MI and hybrid tasks. Generally, the questionnaire results reflected objectively that the subjects considered that performing the proposed hybrid task was not very difficult and that flickers were still acceptable.

IV. Discussion

In this study, simultaneously modulating the luminance and movement of a visual stimulus (i.e., an image of a hand) for eliciting intermodulation SSVEPs is proposed and used to build a BCI system. This coding approach not only can elicit the intermodulation SSVEPs but can also allow subjects to observe hand grasping movements. In the experiments, subjects were asked to perform the corresponding hand MI while looking at the visual stimulus. Features obtained from the intermodulation SSVEP and MI were fused for target classification. The feasibility of the proposed system was verified for both healthy subjects and stroke patients.

The earliest study on the intermodulation frequency can be traced back to the 1980s [40]. After nearly 40 years of extensive research efforts, the intermodulation frequency has not been used only to clarify the neural mechanisms of high-level visual perception but has also been extended to the BCI field [32]. For instance, the previous studies have demonstrated that simultaneously modulating the luminance and the color of a visual stimulus can provide the intermodulation SSVEP, which can be used for BCI target coding [10]–[41]. However, most of the existing studies have used the low-frequency stimulus to obtain intermodulation SSVEPs. The SSVEP-related studies have proven that a high-frequency stimulus can improve visual comfort [42]. Therefore, this study adopted an on/off flicker of 30 Hz for improving user comfort. As shown in Fig. 5, a high-frequency stimulus can also be used to induce intermodulation SSVEPs. In this study, two targets appeared on the screen at the same time and were modulated using both an on/off flicker (30 Hz) and a hand movement modulation (1 Hz or 1.5 Hz). To the best of the authors' knowledge, this study proposes an approach to obtain the intermodulation SSVEP with motion information for the first time. The high classification accuracy obtained for both healthy subjects and stroke patients has validated the feasibility of the proposed coding method.

In the experiments, the subjects were instructed to execute the corresponding hand MI while focusing on the visual stimulus. Thus, each target was encoded by two features, namely, the MI and intermodulation SSVEP features. The proposed system represents a hybrid BCI system combining the MI and intermodulation SSVEP. The SSVEP is a passive response evoked by a visual stimulus reflected in the frequency domain, whereas the ERD/ERS is an active change in the signal energy while imagining a movement. Thus, these two features have different physiological mechanisms and can be used simultaneously with less mutual interference. However, the SSVEP can be evoked and detected with less training, whereas performing the MI tasks to obtain reliable ERD/ERS patterns is difficult for most new users. Therefore, supplementing the SSVEP feature could effectively reduce the BCI illiteracy [26]. These characteristics make the proposed system more robust and applicable to a wider range of users. The obtained results in the comparative experiment have proven that reliable MI and SSVEP signals can be detected simultaneously and that the proposed MI+SSVEP BCI system has certain advantages over the MI- and SSVEP-BCI, especially for the participants who were naïve to the BCI experiments. The high classification accuracy has further verified the feasibility and robustness of the proposed system.

The proposed system was tested for both healthy subjects and stroke patients. The proposed system was tested for stroke patients to explore its application prospect for patient rehabilitation. A system or device used for rehabilitation exercises should sense the movement intention of patients and facilitate them to undertake a prescribed motion [35]. Therefore, providing accurate control commands according to the patients' intentions is crucial. Although the average accuracy of the proposed system declined when it was applied on patients, its accuracy was still significantly higher than the random probability. The performance decline could be caused by the following factors. First, stroke patients have suffered brain damage in a different brain region and to a different degree, which could reduce the quality of data when performing a hybrid task and affect the ability to control a BCI system [43]. It has been found that these patients might elicit weaker intermodulation SSVEPs in most trials. Brain damage also influences the formation of classical cortical activation patterns (i.e., ERD/ERS), so patients might be unable to voluntarily perform the MI tasks, or their contralesional hemispheres might compensate for the motor functions of the lesioned cortex [44]. Second, the patients participating in the experiment had an average age of 62 years. Therefore, except for the brain damage caused by a stroke, physiological changes that come with normal aging could also cause a decline in the BCI accuracy for elder stroke patients [45], [46]. Lastly, the patients were inexperienced with any BCI paradigms, and several of them had post-stroke aphasic. Therefore, it could be hard for some of them to perform the task according to the requirements.

In the following research, the online experiment performance of stroke patients could be improved in certain aspects. Primarily, the mission duration could be extended depending on patients' conditions for achieving higher accuracy. Further, the classification algorithms could be made more patient-friendly. Namely, certain data-based operations could be added to the classification algorithms, such as disease-based channel selection or trial selection for model training. Moreover, sometimes the fusion model could not handle some extreme cases well, namely the accuracy using features of a single modality was nearly random probability. The fusion accuracy could not be effectively promoted. Improving the existed fusion model to ensure the superiority of fusion or applying a general algorithm framework that can process any one of MI, SSVEP, and fusion signals could also be indispensable work

in the future. Finally, implementing a supervised algorithm into the SSVEP classification could be necessary for stroke patients. By re-analyzing the patients' online data using the TDCA [13] for the SSVEP classification, the fusion accuracy increased to 79.89 ± 10.82%. This indicates that the proposed system still has room for improvement for stroke patients. Similarly, the fusion accuracy in the online verification experiment on healthy subjects were 97.88 ± 1.95%. There was an obvious ceiling effect leading to the low contribution of the MI feature to the fusion classification. However, from another perspective, the proposed system shows great potential for expanding the number of targets based on its own paradigm.

In addition to possible improvements in the proposed method, further possibilities of the proposed paradigm could also be explored in future work. Considering a high classification accuracy of a supervised algorithm for the SSVEP signal in a two-class BCI, the number of MI commands could be extended with the help of the SSVEP features by combining the luminance frequency and movement frequency from the left- and right-hand grasping motion to the movement of other limbs, such as the movement of the feet, or finer limb movements, including the waving of the forearm, and even the movement of the fingers. In addition, further improvements in the proposed system's performance could be achieved by introducing other modalities, such as selective sensation [47], without increasing the complexity of the hybrid task.

V. Conclusion

In this study, an innovative approach is proposed to induce intermodulation SSVEPs. The online experiment performance has verified that the proposed encoding approach, which assigns the combinations of luminance frequency and different movement frequency for each target, can elicit stable intermodulation SSVEPs and thus is suitable for BCI system design. In the experimental task, when the subjects focused their attention on the visual stimuli, they were asked to image their own hands participating in grasping movements. The results indicate that visual stimuli help subjects to complete the MI task better. To make full use of features of intermodulation SSVEPs and MI to improve the classification accuracy, this study proposes a fusion algorithm that combines the two features. The online experiment has validated the feasibility of the proposed system for both healthy people and stroke patients. The proposed paradigm might provide an inspiring viewpoint for the MI-BCI with a multi-class or fine imagination movement, which could be helpful for the rehabilitation of patients with movement disorders. In addition, the proposed paradigm could provide the foundation for other multi-modal BCI construction for practical BCI systems.

References

[1] J. Wolpaw, N. Birbaumer, D. McFarland, G. Pfurtscheller, and T. Vaughan, "Brain–computer interfaces for communication and control," *Clin. Neurophys.*, vol. 113, no. 6, pp. 767–791, 2002.

[2] M. Rashid *et al.*, "Current status, challenges, and possible solutions of EEG-based brain–computer interface: A comprehensive review," *Frontiers Neurorobotics*, vol. 14, pp. 14–25, Jun. 2020.

[3] A. Kawala-Sterniuk *et al.*, "Summary of over fifty years with brain–computer interfaces—A review," *Brain Sci.*, vol. 11, no. 1, p. 43, Jan. 2021.

[4] G. Pfurtscheller *et al.*, "The hybrid BCI," *Frontiers Neurosci.*, vol. 21, pp. 4–30, Apr. 2010.

[5] X. Chen, Y. Wang, S. Zhang, S. Xu, and X. Gao, "Effects of stimulation frequency and stimulation waveform on steady-state visual evoked potentials using a computer monitor," *J. Neural Eng.*, vol. 16, no. 6, Oct. 2019, Art. no. 066007.

[6] M.-H. Lee *et al.*, "EEG dataset and openBMI toolbox for three BCI paradigms: An investigation into BCI illiteracy," *GigaScience*, vol. 8, no. 5, p. giz002, May 2019.

[7] X. Chen, Y. Wang, M. Nakanishi, X. Gao, T.-P. Jung, and S. Gao, "High-speed spelling with a noninvasive brain–computer interface," *Proc. Nat. Acad. Sci. India A, Phys. Sci.*, vol. 112, no. 44, pp. E6058–E6067, Nov. 2015.

[8] R. J. M. G. Tello, S. M. T. Müller, A. Ferreira, and T. F. Bastos, "Comparison of the influence of stimuli color on steady-state visual evoked potentials," *Res. Biomed. Eng.*, vol. 31, no. 3, pp. 218–231, Sep. 2015.

[9] S. Ge *et al.*, "SSVEP-based brain–computer interface with a limited number of frequencies based on dual-frequency biased coding," *IEEE Trans. Neural Syst. Rehabil. Eng.*, vol. 29, pp. 760–769, 2021.

[10] X. Chen, Y. Wang, S. Zhang, S. Gao, Y. Hu, and X. Gao, "A novel stimulation method for multi-class SSVEP-BCI using intermodulation frequencies," *J. Neural Eng.*, vol. 14, no. 2, Apr. 2017, Art. no. 026013.

[11] X. Chen, Y. Wang, S. Gao, T.-P. Jung, and X. Gao, "Filter bank canonical correlation analysis for implementing a high-speed SSVEP-based brain–computer interface," *J. Neural Eng.*, vol. 12, no. 4, Jun. 2015, Art. no. 046008.

[12] M. Nakanishi, Y. Wang, X. Chen, Y. Wang, X. Gao, and T.-P. Jung, "Enhancing detection of SSVEPs for a high-speed brain speller using task-related component analysis," *IEEE Trans. Biomed. Eng.*, vol. 65, no. 1, pp. 104–112, Jan. 2018.

[13] B. Liu, X. Chen, N. Shi, Y. Wang, S. Gao, and X. Gao, "Improving the performance of individually calibrated SSVEP-BCI by task-discriminant component analysis," *IEEE Trans. Neural Syst. Rehabil. Eng.*, vol. 29, pp. 1998–2007, 2021.

[14] X. Chen, N. Hu, Y. Wang, and X. Gao, "Validation of a brain–computer interface version of the digit symbol substitution test in healthy subjects," *Comput. Biol. Med.*, vol. 120, May 2020, Art. no. 103729.

[15] A. M. Norcia, L. G. Appelbaum, J. M. Ales, B. R. Cottereau, and B. Rossion, "The steady-state visual evoked potential in vision research: A review," *J. Vis.*, vol. 15, no. 6, p. 4, May 2015.

[16] Y. Jeon, C. S. Nam, Y.-J. Kim, and M. C. Whang, "Event-related (De)synchronization (ERD/ERS) during motor imagery tasks: Implications for brain–computer interfaces," *Int. J. Ind. Ergonom.*, vol. 41, no. 5, pp. 428–436, Sep. 2011.

[17] T. Carlson and J. Del R Millan, "Brain-controlled wheelchairs: A robotic architecture," *IEEE Robot. Autom. Mag.*, vol. 20, no. 1, pp. 65–73, Mar. 2013.

[18] K. LaFleur, K. Cassady, A. Doud, K. Shades, E. Rogin, and B. He, "Quadcopter control in three-dimensional space using a noninvasive motor imagery-based brain–computer interface," *J. Neural Eng.*, vol. 10, no. 4, Aug. 2013, Art. no. 046003.

[19] J. Meng, S. Zhang, A. Bekyo, J. Olsoe, B. Baxter, and B. He, "Non-invasive electroencephalogram based control of a robotic arm for reach and grasp tasks," *Sci. Rep.*, vol. 6, no. 1, pp. 1–15, Dec. 2016.

[20] G. Pfurtscheller, T. Solis-Escalante, R. Ortner, P. Linortner, and G. R. Müller-Putz, "Self-paced operation of an SSVEP-based orthosis with and without an imagery-based 'brain switch': A feasibility study towards a hybrid BCI," *IEEE Trans. Neural Syst. Rehabil. Eng.*, vol. 18, no. 4, pp. 409–414, Aug. 2010.

[21] A. M. Savić, N. M. Malešević, and M. B. Popović, "Feasibility of a hybrid brain–computer interface for advanced functional electrical therapy," *Sci. World J.*, vol. 2014, pp. 1–11, Jan. 2014.

[22] W. Li *et al.*, "A human-vehicle collaborative simulated driving system based on hybrid brain–computer interfaces and computer vision," *IEEE Trans. Cognit. Develop. Syst.*, vol. 10, no. 3, pp. 810–822, Sep. 2018.

[23] N. Yan *et al.*, "Quadcopter control system using a hybrid BCI based on off-line optimization and enhanced human-machine interaction," *IEEE Access*, vol. 8, pp. 1160–1172, 2020.

[24] Z. Wang, Y. Yu, M. Xu, Y. Liu, E. Yin, and Z. Zhou, "Towards a hybrid BCI gaming paradigm based on motor imagery and SSVEP," *Int. J. Hum.-Comput. Interact.*, vol. 35, no. 3, pp. 197–205, 2019.

[25] B. Z. Allison, C. Brunner, V. Kaiser, G. R. Müller-Putz, C. Neuper, and G. Pfurtscheller, "Toward a hybrid brain–computer interface based on imagined movement and visual attention," *J. Neural Eng.*, vol. 7, no. 2, Apr. 2010, Art. no. 026007.

[26] C. Brunner *et al.*, "Improved signal processing approaches in an offline simulation of a hybrid brain–computer interface," *J. Neurosci. Methods*, vol. 188, no. 1, pp. 165–173, Apr. 2010.
[27] T. Yu *et al.*, "Enhanced motor imagery training using a hybrid BCI with feedback," *IEEE Trans. Biomed. Eng.*, vol. 62, no. 7, pp. 1706–1717, Jul. 2015.
[28] L. Ko, O. Komarov, and S.-C. Lin, "Enhancing the hybrid BCI performance with the common frequency pattern in dual-channel EEG," *IEEE Trans. Neural Syst. Rehabil. Eng.*, vol. 27, no. 7, pp. 1360–1369, Jul. 2019.
[29] D. Yang, T.-H. Nguyen, and W.-Y. Chung, "A synchronized hybrid brain–computer interface system for simultaneous detection and classification of fusion EEG signals," *Complexity*, vol. 2020, pp. 1–11, Jun. 2020.
[30] D.-O. Won, H.-J. Hwang, S. Dähne, K.-R. Müller, and S.-W. Lee, "Effect of higher frequency on the classification of steady-state visual evoked potentials," *J. Neural Eng.*, vol. 13, no. 1, Dec. 2015, Art. no. 016014.
[31] Y. Wang, R. Wang, X. Gao, B. Hong, and S. Gao, "A practical VEP-based brain–computer interface," *IEEE Trans. Neural Syst. Rehabil. Eng.*, vol. 14, no. 2, pp. 234–240, Jun. 2006.
[32] N. Gordon, J. Hohwy, M. J. Davidson, J. J. A. van Boxtel, and N. Tsuchiya, "From intermodulation components to visual perception and cognition—A review," *NeuroImage*, vol. 199, pp. 480–494, Oct. 2019.
[33] J.-R. Duann and J.-C. Chiou, "A comparison of independent event-related desynchronization responses in motor-related brain areas to movement execution, movement imagery, and movement observation," *PLoS ONE*, vol. 11, no. 9, Sep. 2016, Art. no. e0162546.
[34] T. Higashi *et al.*, "A method for using video presentation to increase the vividness and activity of cortical regions during motor imagery tasks," *Neural Regener. Res.*, vol. 16, no. 12, pp. 2431–2437, Dec. 2021.
[35] P. D. Baniqued *et al.*, "Brain–computer interface robotics for hand rehabilitation after stroke: A systematic review," *J. Neuroeng. Rehabil.*, vol. 18, no. 1, p. 15, Jan. 2021.
[36] D. H. Brainard, "The psychophysics toolbox," *Spatial Vis.*, vol. 10, no. 4, pp. 433–436, 1997.
[37] P. Chholak *et al.*, "Visual and kinesthetic modes affect motor imagery classification in untrained subjects," *Sci. Rep.*, vol. 9, no. 1, p. 9838, Dec. 2019.
[38] F. Lotte and C. Guan, "Regularizing common spatial patterns to improve BCI designs: Unified theory and new algorithms," *IEEE Trans. Biomed. Eng.*, vol. 58, no. 2, pp. 355–362, Feb. 2011.
[39] S. Lemm, B. Blankertz, G. Curio, and K. R. Müller, "Spatio-spectral filters for improving the classification of single trial EEG," *IEEE Trans. Biomed. Eng.*, vol. 52, no. 9, pp. 1541–1548, Sep. 2005.
[40] V. Zemon and F. Ratliff, "Visual evoked potentials: Evidence for lateral interactions," *Proc. Nat. Acad. Sci. India A, Phys. Sci.*, vol. 79, no. 18, pp. 5723–5726, Sep. 1982.
[41] X. Chen, Z. Chen, S. Gao, and X. Gao, "Brain–computer interface based on intermodulation frequency," *J. Neural Eng.*, vol. 10, no. 6, Dec. 2013, Art. no. 066009.
[42] P. F. Diez, V. A. Mut, E. M. A. Perona, and E. L. Leber, "Asynchronous BCI control using high-frequency SSVEP," *J. Neuroeng. Rehabil.*, vol. 8, p. 39, Jul. 2011.
[43] M. Bamdad, H. Zarshenas, and M. A. Auais, "Application of BCI systems in neurorehabilitation: A scoping review," *Disab. Rehabil., Assistive Technol.*, vol. 10, no. 5, pp. 355–364, 2015.
[44] X. Shu *et al.*, "Fast recognition of BCI-inefficient users using physiological features from EEG signals: A screening study of stroke patients," *Frontiers Neurosci.*, vol. 12, p. 93, Feb. 2018.
[45] I. Volosyak, F. Gembler, and P. Stawicki, "Age-related differences in SSVEP-based BCI performance," *Neurocomputing*, vol. 250, pp. 57–64, Aug. 2017.
[46] M. L. Chen, D. Fu, J. Boger, and N. Jiang, "Age-related changes in vibro-tactile EEG response and its implications in BCI applications: A comparison between older and younger populations," *IEEE Trans. Neural Syst. Rehabil. Eng.*, vol. 27, no. 4, pp. 603–610, Apr. 2019.
[47] L. Yao, J. Meng, D. Zhang, X. Sheng, and X. Zhu, "Combining motor imagery with selective sensation toward a hybrid-modality BCI," *IEEE Trans. Biomed. Eng.*, vol. 61, no. 8, pp. 2304–2312, Aug. 2014.